Journal of Catalysis 257 (2008) 244–254

Contents lists available at ScienceDirect

Journal of Catalysis

www.elsevier.com/locate/jcat

# Development of a transient response technique for heterogeneous catalysis in the liquid phase, Part 1: Applying an electrospray ionization mass spectrometry (ESI-MS) detector

D. Radivojević [a,1], M. Ruitenbeek [b], K. Seshan [a], L. Lefferts [a,*]

[a] Catalytic Processes and Materials, Faculty of Science and Technology, Institute of Mechanics, Processes and Control Twente (IMPACT) and MESA+, University of Twente, P.O. Box 217, 7500AE Enschede, The Netherlands

[b] SABIC Europe R&D, P.O. Box 319, 6160 AH, Geleen, The Netherlands

ARTICLE INFO

*Article history:*
Received 12 February 2008
Revised 29 April 2008
Accepted 1 May 2008
Available online 10 June 2008

*Keywords:*
Transient operated reactor
Liquid phase
ESI-MS
Glucose oxidation
Nitrite hydrogenation

ABSTRACT

We have developed a novel, transient response technique for liquid-phase heterogeneous catalytic studies, equipped with an electrospray ionization mass spectrometry (ESI-MS) detector. The technique was successfully applied as an online method for real-time detection of species dissolved in aqueous product streams at the exit of a catalytic reactor. Two test reactions, nitrite reduction with $Pt/SiO_2$ and glucose oxidation with Pt/CNF/Ni, were used to demonstrate semi-quantitative monitoring of reactants, intermediates, and products. The capability of the novel technique is demonstrated by the fact that the ESI-MS detector is sufficiently sensitive to determine quantitatively extreme small amounts of physisorbing nitrite, down to 0.5% of a monolayer on the Pt surface. Nitrite also reacts with preadsorbed hydrogen, and the quantitative experimental results agree with the formation of both nitrogen and ammonia. The ESI-MS detector is able to distinguish between different components simultaneously, as in the case of glucose oxidation; this is its most significant advantage over existing transient techniques. A limitation of ESI-MS is its inability to detect gases dissolved in liquids, due to the relatively mild ionization process through electrospray. The second part of this article discusses an alternative detector to satisfy this deficiency.



## 1. Introduction

Heterogeneous catalytic reactions in the liquid phase are important in such areas as production of bulk chemicals, fine chemicals, and pharmaceuticals [1,2]. It is well known that in most cases, production of fine chemicals and pharmaceuticals is less efficient compared with that of bulk chemicals, due to multistep synthesis procedures and the use of stoichiometric reduction and oxidation reactions. Therefore, efficient and selective catalysts are needed to improve these processes. Many of the targeted molecules are relatively complex and have limited thermal stability, implying that most of the reactions require solvents.

The development of highly efficient catalysts for gas-phase reactions has been assisted by powerful characterization techniques, in situ characterization [3] and transient techniques for mechanistic studies [4–6]. Transient methods were significantly optimized by Gleaves et al. [7] when developing the temporary analysis of products (TAP) method, which has been recently used by many researchers, including Yablonsky et al. [8] and Nijhuis et al. [9]. A similar approach is appropriate for developing and improving catalysts for application in the liquid phase. However, many of the experimental techniques developed for gas-phase experiments require vacuum or low pressure and cannot be applied in the liquid phase. An example of successful modification of a characterization technique to enable experiments in the liquid phase is infrared (IR) spectroscopy in attenuated total reflection (ATR) mode, which was pioneered by Bürgi et al. [10] and further developed by Ebbesen et al. [11].

In transient experiments, including chemisorption experiments in pulse mode or step change mode, there are no major problems when operating in the liquid phase. The challenge is mostly technical in nature, because rapid analysis of species at the exit of the reactor is required for transient studies. In gas-phase transient experiments, this is normally achieved by online mass spectrometry (MS), which allows real-time multicomponent analysis at least semiquantitatively. The goal of the present study is to develop and demonstrate a similar technique that can be used for heterogeneous catalytic experiments in the liquid phase.

Previous attempts have been made to perform transient-type experiments in the liquid phase. A refractive index (RI) detector

* Corresponding author. Fax: +31 53 489 4683.
*E-mail address:* l.lefferts@tnw.utwente.nl (L. Lefferts).

[1] Present address: SABIC Europe R&D, P.O. Box 319, 6160 AH, Geleen, The Netherlands.

0021-9517/$ – see front matter 
doi:10.1016/j.jcat.2008.05.002

was used in a few studies [12,13]. Denayer et al. [12] performed pulse-type transient experiments to determine the influence of polarity, pore size, and topology on the adsorption of *n*-alkanes, isoalkanes, aromatics, and other organic components on FAU and MFI zeolites. These authors used a high-performance liquid chromatography (HPLC) cartridge filled with FAU or MFI zeolites, combined with an inline differential RI detector. Jonker et al. [13] used tracer pulse experiments to determine an effective diffusion coefficient, $D_e$, of edible oils and their fatty acid methyl esters over $Ni/SiO_2$ catalysts. These authors also used an HPLC cartridge filled with catalyst (5–40 μm) as reactor, combined with an inline differential RI detector. Continuous-flow UV–visible (UV–vis) spectroscopy detectors also have been used [14–16]. Hejtmánek et al. [14] performed step-type transient experiments to determine axial dispersion coefficients for tracer/carrier–liquid systems, such as acetone–water, toluene–methanol, and acetone–ethylene glycol, using HPLC cartridges filled with 4.5 μm of monodispersed spherical glass particles. Lin et al. [15] performed tracer studies using liquid chromatography to determine effective intraparticle diffusion coefficients and adsorption equilibrium constants on silicalite and alumina of various alcohols in water and of toluene, acetone, and ethyl acetate dissolved in cyclohexane. Kiraly et al. [16] used an HPLC cartridge filled with a $Pt/Al_2O_3$ catalyst in transient pulse experiments to determine Pd dispersion at the solid–liquid interface. Gao et al. [17] used a flow-through liquid cell for Fourier transform infrared spectroscopy (FTIR) analysis, connected to an HPLC cartridge filled with 55-μm $Pt/Al_2O_3$ catalyst particles to study the hydrogenation of acetophenone.

All of these examples have in common that the equipment consists of (i) a liquid feed section equipped with a device to generate pulses or steps, (ii) a catalytic reactor based mainly on HPLC cartridges filled with catalyst, and (iii) a detector. The most significant difference is the choice of detector. Commonly used detectors (e.g., RI, UV–vis [18]) have the disadvantage of not being able to distinguish between different compounds. This is a serious limitation when more then one component is present in the mixture leaving the reactor. Consequently, we have developed alternative methods for detecting different species leaving the reactor simultaneously, based on electrospray ionization mass spectrometry (ESI-MS). Mass spectrometry is a fast technique that in principle is able to detect multiple components simultaneously [19], although this is not trivial. Mass spectrometers with electrospray ionization are available commercially as part of HPLC-MS systems equipped with a liquid-phase–MS interface [20]. To the best of our knowledge, a transient response technique for liquid-phase heterogeneous catalytic studies equipped with an ESI-MS as detector has not been described previously.

The pressure drop in the catalytic reactor has been minimized in this study to generate sufficient flexibility to optimize liquid flow rates. The first approach was to use a catalyst based on monodispersed silica support particles (Microsorb silica) [21]. The second approach was to use carbon nanofibers (CNFs) supported on Ni (CNF/Ni) [22] foam as a catalyst support with extreme high porosity.

To develop and demonstrate our technique, we selected two catalytic reaction systems in aqueous phase studied previously by our group: (i) catalytic reduction of nitrite ($NO_2^-$) over a $Pt/SiO_2$ catalyst and (ii) catalytic oxidation of glucose over Pt supported on carbon. Nitrite hydrogenation [23] is a relevant reaction for both nitrate-to-nitrogen denitrification of drinking water [24] and nitrate hydrogenation to hydroxyl-amine, an intermediate in the production of caprolactam [1]. Oxidative conversion of glucose is important in view of the anticipated shift toward renewable feedstocks for the chemical industry. Glucose can be upgraded to a more valuable compound, such as gluconic acid, a building block for production of chelating agents [25–27]. Therefore, we developed the technique for application in the aqueous phase, knowing that many other processes in organic solvents could benefit as well.

## 2. Experimental

### 2.1. Materials

HPLC silica (Microsorb from Varian, BET surface area 198 $m^2/g$; mean particle size 5 μm) was used as the support for $Pt/SiO_2$. The fixed-bed reactor was created by filling an HPLC cartridge ($4.6 \times 10^{-3}$ m i.d., 0.1 m long) with $Pt/SiO_2$ catalyst. The catalyst bed was fixed in the cartridge with two metallic 2-μm frits at the inlet and the outlet. CNF/Ni foam was prepared as described elsewhere [22,28]. The CNF loading was 30 wt%, and the total surface area was 50 $m^2/g$ (BET, Micromeritics). Pt/CNF supported on Ni foam was obtained in cylindrical pieces ($4.55 \times 10^{-3}$ m wide, $5 \times 10^{-3}$ m long).

Tetra ammonium–platinum hydroxide $(NH_3)_4Pt(OH)_2$ (99.9%, Aldrich) was used as the platinum precursor for the $SiO_2$ supported catalyst, whereas $Pt(C_5H_7O_2)_2$ (99%, Aldrich) was used as the platinum precursor for CNF. Ultra-pure LC-MS grade water (Biosolve) was used to prepare $(NH_3)_4Pt(OH)_2$, $NaNO_2$ (99%, Aldrich), glucose (99%, Aldrich), and gluconic acid (50% aqueous solution, Aldrich) solutions. Toluene (99%, Merck) was used to prepare solutions of $Pt(C_5H_7O_2)$. Argon (Air Products BIP, 99.9999%) was further purified using an oxygen trap (OxyTrap, Alltech) to decrease the oxygen content to $\leqslant$10 ppb. Hydrogen (99.999%) and oxygen (99.999%) were purchased from Indugas.

### 2.2. Catalyst preparation and characterization

The $Pt/SiO_2$ catalyst was prepared by an ion-exchange method [21]. The platinum loadings of fresh and spent catalysts were determined with X-ray fluorescence spectroscopy (XRF; Phillips PW 1480 spectrometer). The Pt/CNF/Ni catalyst was created by wet impregnation in the following sequence. First, 0.9 g of CNF/Ni was contacted overnight with 60 mL of $Pt(C_5H_2O_7)_2$ in toluene. Then the CNF/Ni pieces were dried for 3 h at 60 °C in a rotary evaporator, followed by calcination at 270 °C for 2 h in 20% $O_2$ in $N_2$ and reduction in 20% $H_2$ in $N_2$ for 1 h. The flow rate of gases during treatment was 100 ml $min^{-1}$. The Pt concentration of the Pt/CNF/Ni catalyst could not be determined with XRF because the foam did not fit into the XRF spectrometer; however, the amount of platinum introduced should result in 3% by weight.

Platinum dispersions of the $Pt/SiO_2$ and Pt/CNF/Ni catalysts were measured with a pulse-flow chemisorption apparatus (ChemiSorb 2750, Micromeritics). The platinum metal dispersion was calculated assuming a $H:Pt_s$ ratio of unity [29]. Particle sizes of fresh $Pt/SiO_2$ and Pt/CNF/Ni catalysts were cross-checked with transmission electron microscopy (TEM; Phillips CM 30 microscope, 300 kV); typically, the sizes of 100 platinum particles were determined in each sample.

### 2.3. Transient response experimental setup

Fig. 1 presents a schematic representation of the equipment for the experiments. The setup consisted of (i) a feed section (containers, selection valve and pump) with a switching valve to introduce a well-shaped step/pulse function in the reactant concentration; (ii) a catalytic reactor, (i.e., packed bed or filled with foam); and (iii) an ESI-MS detector connected directly to the reactor outlet.

#### 2.3.1. Feed section with pulse/step introducing device

Gas-tight liquid containers (three homemade 1.8-L vessels made of Pyrex glass) were connected to a pulse-free HPLC binary pump

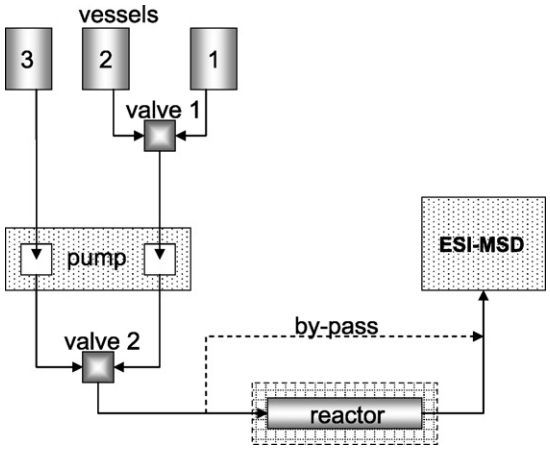


**Fig. 1.** Scheme of the experimental set-up.

(G1312A, Agilent) with 1/8″ tubings (Swagelock), either directly (container 3, containing pure water) or through an HPLC valve 1 (G1160A, Agilent) (containers 1 and 2, containing dissolved gases and/or with reacting species). The containers were stirred electromagnetically. Gas was supplied to the liquid containers through glass frits positioned close to the stirrer. The HPLC pump yielded flow rates in the range 0.2–0.5 ml min$^{-1}$ (±1%). Pulse- or step-type changes in the reactant concentrations were introduced by switching HPLC valve 2 (G1158A, Agilent). The system was automated and controlled with Chemstation software, version b 02.01 (Agilent) [20].

### 2.3.2. Reactors

Two types of catalytic reactors—a Pt/$SiO_2$ fixed-bed reactor and Pt/CNF/Ni supported on Ni foam—were used. To prevent channeling of liquid, the cartridge was filled with the Pt/$SiO_2$ catalyst very carefully, following standard procedures for creating HPLC columns [30]. The CNF foam was fitted tightly fitted into the cartridge, and the distance to the wall was in the same range as the pore diameter in the foam ($1–5 \times 10^{-4}$ m). The volume of the voids within the reactors was estimated by weighing the reactors before and after filling them with water. The estimated volume was used to calculate residence time and was always within an error of ±5%. The dynamic behavior of the reactors (filled with silica support or with CNF/Ni support without Pt) was determined by pulsing nitrite solution (concentration $2.2 \times 10^{-4}$ mol dm$^{-3}$, 50 ml for 100 min) or glucose solution (concentration $5.6 \times 10^{-5}$ mol dm$^{-3}$, 12.5 mL for 25 min). An earlier study found that silica leached when alkaline glucose solution was flowed [30]; therefore, we used Pt supported on CNF/Ni for the experiments with glucose.

The catalytic reactor was placed in an oven made of aluminum blocks with two integrated heating fingers (G4A78, Watlow/Kurval). The temperature of the oven was kept uniform at 60 °C (±0.5 °C) by a temperature controller (Eurotherm 2132).

### 2.3.3. Analyzer

Qualitative and quantitative analysis of ionic species present in the effluent from the reactor was performed with an online mass spectrometry detector (MSD) (SL/G1956B, Agilent) equipped with an electrospray ionization (ESI) liquid-phase interface (G1948A, Agilent). The liquid chromatography part of the equipment was removed, and the effluent from the reactor was directly injected into the electron-spray ionization chamber.

The ESI process involves three main steps [31]: (i) production of charged droplets at the ES capillary tip; (ii) shrinkage of the charged droplets by solvent evaporation, leading to very small charged droplets capable of producing gas-phase ions; and (iii) formation of gas-phase ions from charged droplets. Parameters that can affect the ESI process are solvent composition, temperature, spray voltage, solvent flow rate, and nebulizing gas flow rate [32]. ESI is usually applied to analyze high-molecular-weight and polar molecules, like organic acids, which easily form ions. Unfortunately, compounds that are difficult to ionize (e.g., nitrogen and other dissolved gases) cannot be detected with ESI-MS. In the present study, ESI was operated in negative mode, and analysis was performed in the mass range of 10 and 500 m/z. The signal-to-noise ratio was optimized for both cases via the choice of parameters shown in Table 1. Additives usually applied to enhance the ionization process [33] were not used in this study, to prevent any interaction of these additives with the catalyst.

**Table 1**
Instrumental parameters for ESI-MS analysis

| | |
|---|---|
| Capillary voltage (kV) | 4.0/3.8[a] |
| Desolvation gas temperature (°C) | 350 |
| Nebulising gas flow rate (L min$^{-1}$) | 12 |
| Water with analyte flow rate (mL min$^{-1}$) | 0.5 |
| Water flow rate (mL min$^{-1}$) | 0.5 |

[a] Capillary voltage used in experiments with glucose.

### 2.4. Catalytic experiments

Before the experiments, vessels 1 and 3 were filled with approximately 1 L of pure water and vessel 2 was filled with 1 L of aqueous solution containing the reacting species (glucose or nitrite ions). An aqueous solution of NaOH ($1 \times 10^{-3}$ mol) was used to adjust pH of the glucose solution to 9 ± 0.3, to prevent inhibition of the catalysts with carboxylic acids [34]. The liquids in vessels 2 and 3 were flushed with argon to remove any dissolved gases (60 min, 200 ml min$^{-1}$), whereas in vessel 1 water was saturated with oxygen or hydrogen (30 min, 200 ml min$^{-1}$, 22 °C). Experiments were performed with at a flow rate of 0.5 ml min$^{-1}$ at 60 °C.

Pulse titration experiments with aqueous nitrite solution over Pt/$SiO_2$ were performed in the following sequence. First, water saturated with hydrogen (from vessel 1) was flowed for 60 min through the reactor to preadsorb hydrogen. The amount of hydrogen introduced was well in excess of that needed to reach full coverage of the platinum surface. Then pure water (from vessel 3) was flowed through the reactor for 30 min to remove dissolved hydrogen from the solution and physisorbed hydrogen from Pt/$SiO_2$. The results given in Part 2 of this paper (Fig. 2b) demonstrate that 30 min is more than enough time to obtain complete removal. Finally, the preadsorbed hydrogen was contacted with pulses of nitrite solution (concentration $2.2 \times 10^{-4}$ mol dm$^{-3}$, 5 ml for 10 min); pulses were repeated every 20 min, with pure water flowed between pulses.

Another sequence was applied to study the interaction of Pt/CNF/Ni with aqueous glucose solution. First, water saturated with oxygen (from vessel 1) was flowed for 30 min (flow, 0.5 ml min$^{-1}$) at 60 °C through the reactor to preadsorb oxygen. Then pure water (from vessel 1) was flowed through then reactor for 60 min to remove dissolved oxygen from the solution and physisorbed oxygen from Pt/CNF/Ni. Finally, preadsorbed oxygen was contacted with pulses of glucose solution (concentration $5.6 \times 10^{-5}$ mol dm$^{-3}$, 30 ml for 60 min). Pulses were repeated after 20 min, with pure water flowed between pulses. Calibrations for quantitative interpretation are described in next section.

## 3. Results and discussion

We first present and discuss the results of catalyst characterization, then explore pressure drop, response time of the detector, and the hydrodynamic behavior of the reactors. We then describe detection and calibration of species with ESI-MS. Finally, we present

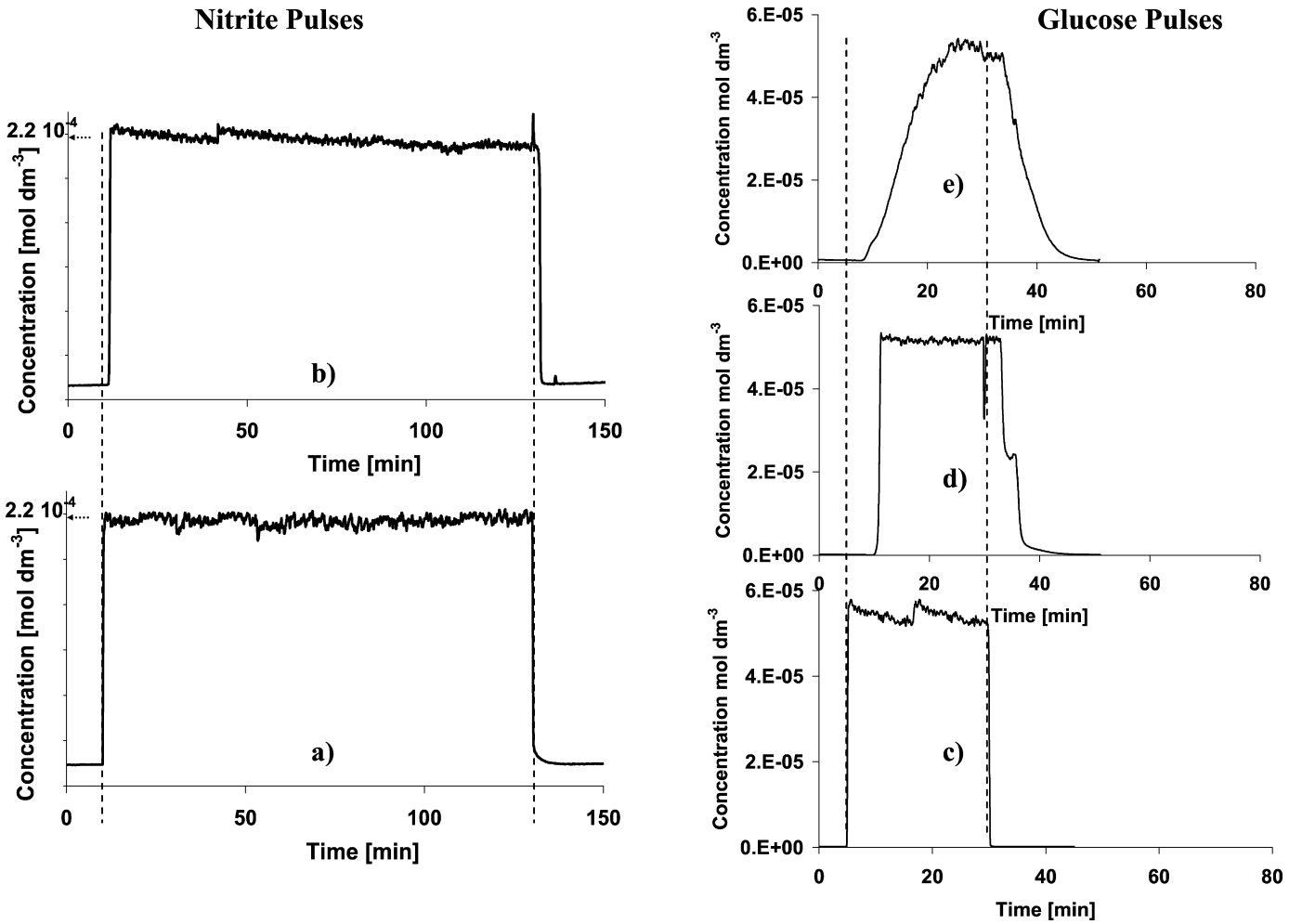


**Fig. 2.** Response of (a) by-pass and (b) reactor with silica to the pulse of nitrite (50 mL during 100 min with flow rate 0.5 ml min$^{-1}$, $c_M$ ($NO_2^-$) = 2.2 × 10$^{-4}$ mol dm$^{-3}$, $T$ = 60 °C). Response of (c) by-pass, (d) column with silica and (e) column with CNF to a pulse of glucose (12.5 ml during 25 min with flow rate 0.5 ml min$^{-1}$, $c_M$ ($C_6H_{12}O_6$) = 5.6 × 10$^{-5}$ mol dm$^{-3}$, $T$ = 60 °C).

**Table 2**
Catalyst loadings and dispersions determined in gas phase

| Catalyst | Loading (wt%) | H/Pt | Amount of Pt | | H/Pt–TEM[a] |
|---|---|---|---|---|---|
| | | | Bulk (μmol/g) | Surface (μmol)[b] | |
| $Pt/SiO_2$ | 1.0 ± 0.05 | 0.65 | 51 | 10.0 | 0.55 |
| Pt/CNF | 3.0[c] | 0.25 | 154 | 11.0 | 0.29 |

[a] Calculated based on: $D(\text{TEM}) = \frac{1.08}{d(nm)}$ [29].

[b] Amount of surface platinum atoms available in the reactor.

[c] The Pt loading assumed based on preparation procedure.

the results of transient catalytic experiments, probing the reactivity of preadsorbed hydrogen with nitrite and preadsorbed oxygen with glucose.

### 3.1. Catalyst preparation and characterization

The platinum loading of $Pt/SiO_2$ (1 ± 0.05 wt%) was in agreement with expectations based on the preparation procedure used (Table 2). Pt/CNF/Ni could not be analyzed with XRF; therefore, the platinum loading according the preparation procedure (3 wt%) was assumed. No contamination could be detected with XRF on all catalysts before or after the experiments. Table 2 also reports the platinum dispersion measured with hydrogen chemisorption (65% for $Pt/SiO_2$ and 25% for Pt/CNF/Ni). The platinum dispersions estimated from the average metal particle size obtained from TEM analysis closely agreed with the hydrogen chemisorption data, indicating that the assumption of the Pt loading of Pt/CNF/Ni is reasonable. In the case of $Pt/SiO_2$, the calculated dispersion based on TEM was slightly lower than that according to chemisorption, indicating that this catalyst may have contained some very small particles (<2 nm) that could not be clearly observed with TEM.

### 3.2. Pressure drop, response time of the detector, and hydrodynamic behavior of the reactors

Flowing 0.5 ml min$^{-1}$ over the $Pt/SiO_2$ packed bed resulted in a typical pressure drop of 40 bar; 2–3 bars is typically due to the two metal frits. After 1 week of operation, the pressure drop increased slightly, from 40 to 43 bars, and remained constant thereafter. This effect may be due to further compaction of the bed. For the same flow rate, the pressure drop over the foam increased from 2 bars initially to 12 bars after 2 weeks of use. During the subsequent 2 weeks of use, the pressure drop remained constant. Inspection of the used reactor showed black CNF fines deposited on the frit at the outlet. After the frit was cleaned, the pressure drop recovered completely, with no new fines or pressure drop were observed. Thus, a small part of the CNFs on Ni foam were not well attached and could be removed by flowing compressed air. This observation agrees well with the results of Jarrah et al. [28,35] who, when describing the preparation of CNFs on Ni foam, reported that a small fraction of the CNFs was loosely attached,

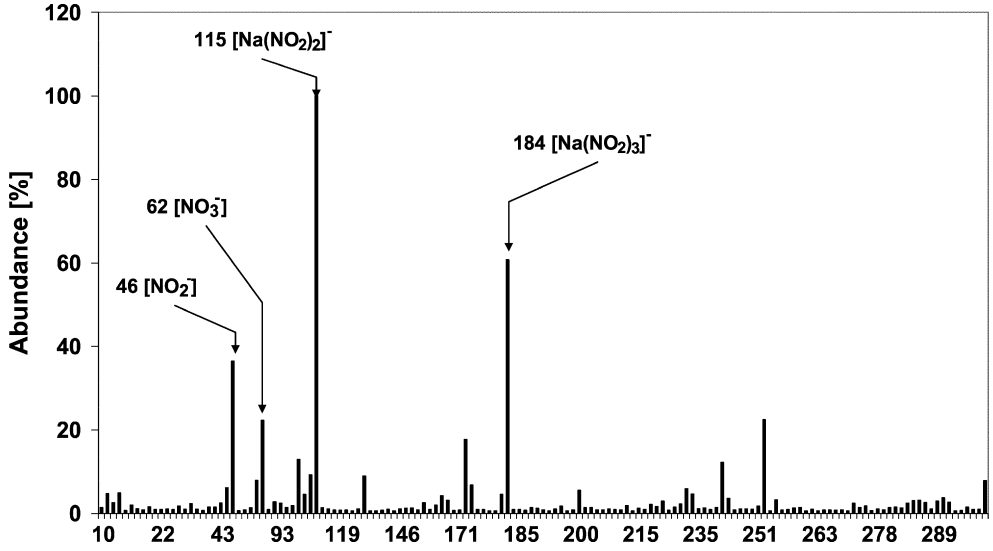


**Fig. 3.** Spectrum obtained during analysis of $2 \times 10^{-4}$ mol dm$^{-3}$ nitrite ($NO_2^-$) aqueous solution at 60 °C and liquid flow rate of 0.5 ml min$^{-1}$.

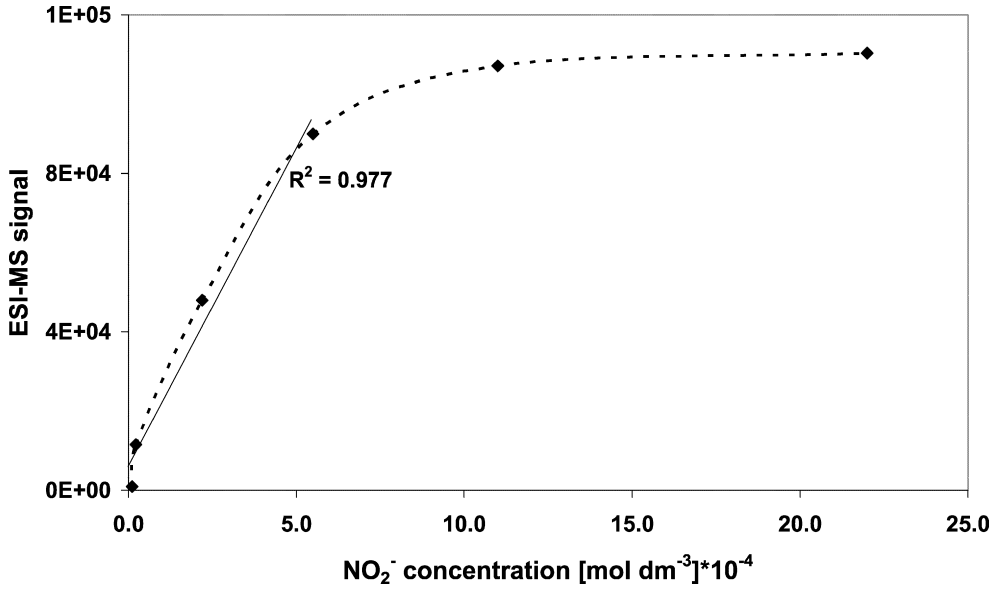


**Fig. 4.** Calibration curve for nitrite (♦—m/zl 15 $[Na(NO_2)_2]^-$) obtained at 60 °C and liquid flow rate of 0.5 ml min$^{-1}$.

whereas the remaining CNFs was strongly bonded to the Ni foam support.

The response time of the detector (i.e., the time required for the signal to reach a level of 95% of the stable value) was on the order of 20 s, as observed in the blank experiment by-passing the reactor for both nitrite ions (Fig. 2a) and glucose (Fig. 2c). Fig. 2 presents the complete response to the pulse.

Fig. 2b shows the response to a nitrite pulse with the $SiO_2$ fixed bed. A delay of 1.45 min was observed, in good agreement with the residence time in the reactor (1.40 min) based on the free volume in the reactor. The breakthrough curve from the reactor with silica was sharp, and the signal stabilized within 20 s (Fig. 2b). The slight decrease in signal during the plateau, as well as the small step after 40 min, were due to process disorder and were not significant. Results from the same experiment with glucose and $SiO_2$ are shown in Fig. 2d. Surprisingly, a delay of 6.10 min was seen at both the front and back ends of the pulse, whereas the residence time remained 1.4 min. The difference between the step response in the blank experiment (Fig. 2c) and in the experiment with silica (Fig. 2d) indicates that about 0.1 μmol of glucose adsorbed reversibly. The shape of the desorption curve indicates two types of adsorbed glucose molecules. Weakly adsorbed glucose desorbed first, reaching a stable concentration in the outlet at a lower level when strongly adsorbed glucose desorbed. Whether this was due to inhomogeneity of the silica surface or lateral interaction between glucose molecules remains unclear.

Fig. 2e shows the response of a reactor with CNF/Ni to a glucose pulse. Stabilization of the signal was attained after 20 min (Fig. 2e), much longer than the residence time of 3 min in the free volume of the CNF/Ni reactor. Furthermore, the shape of the response signal indicates significant back-mixing in the CNF/Ni foam. Therefore, longer pulses were required in this case (see Section 3.5).

### 3.3. Calibration

Fig. 3 shows a typical MS spectrum for a sodium–nitrite solution revealing significant peaks at m/z 46, 115, and 184. Mass m/z 46 corresponds to the $NO_2^-$ anion, whereas m/z 115 and 184 are agglomerates of nitrite and sodium ions [36], that is, $([2NO_2^-]Na^+)^-$ and $([3NO_2^-]2Na^+)^-$, respectively. The most in-

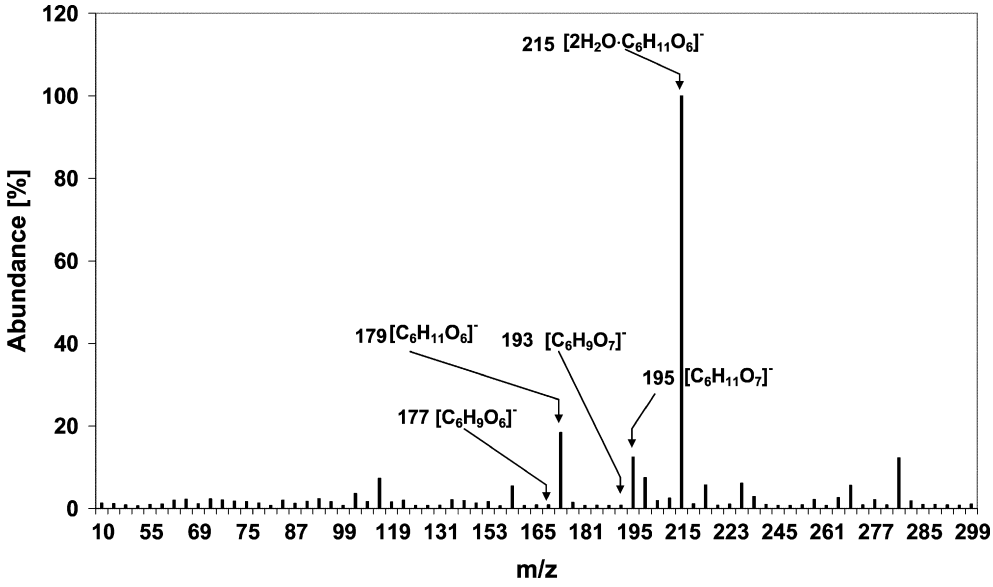


**Fig. 5.** Glucose spectrum for $5.6 \times 10^{-5}$ mol dm$^{-3}$ glucose solution at 60 °C and liquid flow rate of 0.5 ml min$^{-1}$.

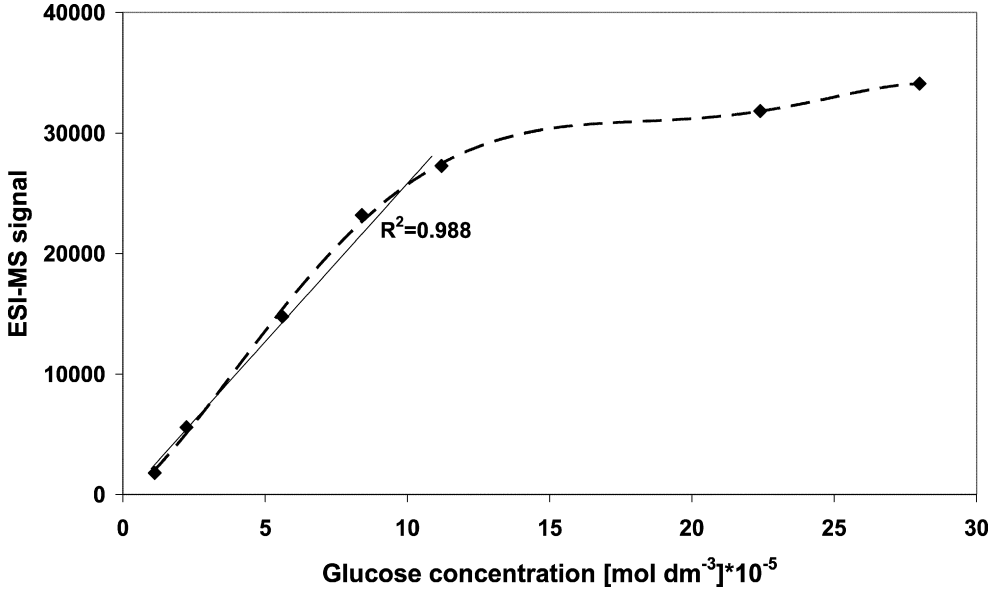


**Fig. 6.** Calibration curve for glucose (m/z 215 − $2H_2O{\cdot}[C_6H_{11}O_6]^-$) obtained at 60 °C and liquid flow rate of 0.5 ml min$^{-1}$.

tense peak (i.e., m/z 115) can be used for quantitative determination, because intensity increases regularly with concentration (Fig. 4); surprisingly, the intensities of m/z 46 and m/z 184 decreased with increasing concentration. The calibration line was calculated using linear regression ($R^2 = 0.977$). This indicates that the m/z values generally must be selected carefully based on calibration experiments. The concentration of nitrite could be accurately determined in the concentration window between $2 \times 10^{-5}$ mol dm$^{-3}$ (detection limit with signal/noise >5) and up to about $5 \times 10^{-4}$ mol dm$^{-3}$; at higher concentrations, the MS signal showed little further increase (Fig. 4). This is a saturation effect [37] caused by a decrease of the ionization efficiency. Ammonia is, along with nitrogen, a product from the hydrogenation of nitrite. Unfortunately, ammonia could not be detected due to the low molecular mass. On the other hand, we verified that the presence of ammonia did not affect the calibration of nitrite.

Fig. 5 shows a typical spectrum for glucose. The most significant peaks can be seen at m/z 215 and 179. The peak at m/z 215 corresponds to the deprotonated glucose ion with two associated molecules of water ($2H_2O{\cdot}[C_6H_{11}O_6]^-$) and is the most suitable for quantitative determinations, because the calibration curve for this peak increased linearly with increasing glucose concentration (Fig. 6). The calibration line was calculated using linear regression ($R^2 = 0.988$). The peak at m/z 179 corresponded to $[C_6H_{11}O_6]^-$ (i.e., deprotonated glucose molecule without water); this signal could not be used here, because it did not increase regularly with increasing glucose concentrations. We cannot rule out the presence of gluconic acid contamination because of the peak at m/z 195; however, this signal also could be due to fragmentation of glucose during ionization. The limit of detection for glucose was $5.6 \times 10^{-6}$ mol dm$^{-3}$, and the glucose concentration could be accurately determined up to $1 \times 10^{-4}$ mol dm$^{-3}$, before the saturation effect occurred (Fig. 6).

Calibration also was done for gluconic acid (Fig. 7); the most significant signal observed was at m/z 195, corresponding to deprotonated gluconic acid $[C_6H_{11}O_7]^-$ anion. The calibration line was calculated using linear regression ($R^2 = 0.952$). Gluconic acid could be accurately determined between $1 \times 10^{-6}$ up to $1 \times$

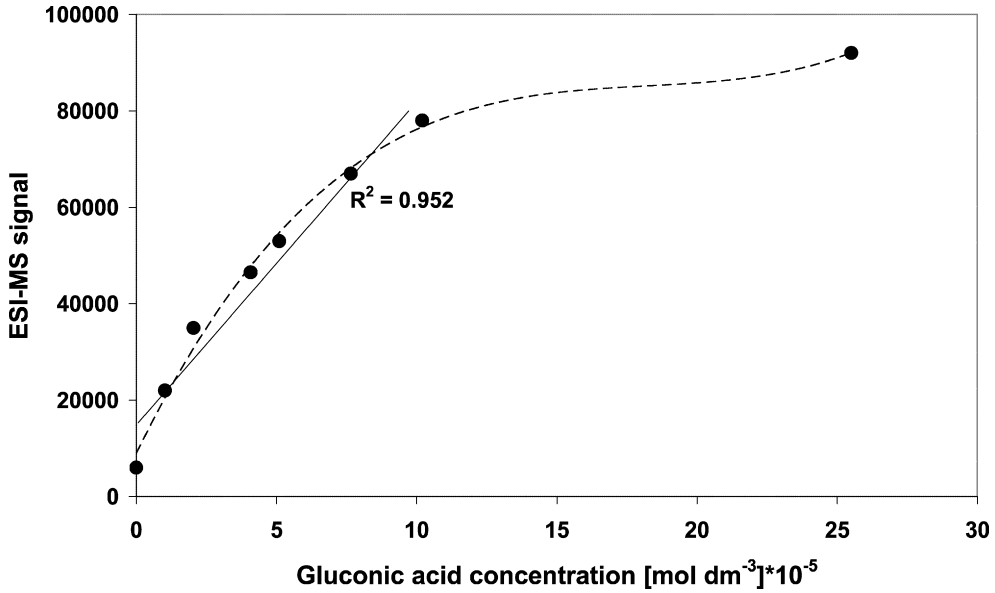


**Fig. 7.** Calibration curve for gluconic acid (m/z 195 − $[C_6H_{11}O_7]^-$) obtained at 60 °C and liquid flow rate of 0.5 ml $min^{-1}$.

$10^{-4}$ mol $dm^{-3}$. Experiments with mixtures of glucose ($5.6 \times 10^{-5}$ mol $dm^{-3}$) and gluconic acid ($5.1 \times 10^{-5}$ mol $dm^{-3}$) revealed some charge competition; that is, the glucose concentration was underestimated, whereas the gluconic acid concentration was overestimated. The error in both cases was a maximum of 20%, which we currently accept as the limit of experimental inaccuracy at this stage of development.

Calibrations were repeated every 2 weeks, resulting in reproducible results with 10% error. Applying the ESI-MS detector in the continuous-flow mode caused frequent blockage of the nebulizing needle, due to deposition of dissolved species on the wall of the needle (especially during the analysis of nitrite). This was manifested by the pressure rise in the ESI (2–3 bars after 1 month of operation). This effect was prevented by daily cleaning and replacement of the nebulizing needle when pressure started to rise.

### 3.4. Catalytic reduction of nitrite species over $Pt/SiO_2$

Fig. 8a shows the experimental result of pulsing nitrite for both the prereduced $Pt/SiO_2$ catalyst and for the silica support only (which served as a blank experiment). Complete consumption of nitrite occurred during the first pulse on the reduced $Pt/SiO_2$. A breakthrough occurred during the next three pulses. Finally, the surface area of the peaks became identical to that seen in the blank experiment, indicating no further hydrogen consumption. The total amount of nitrite converted was 2.4 μmol.

Selective hydrogenation of nitrite with hydrogen preadsorbed on platinum under the present experimental conditions resulted in formation of nitrogen and ammonia, according the following equations [38]:

$$2NO_2^- + 6H_a = N_2 + 2OH^- + 2H_2O \quad (1)$$

and

$$NO_2^- + 6H_a = NH_4^+ + 2OH^-. \quad (2)$$

The total amount of hydrogen available, adsorbed on the Pt catalyst, was 10 μmol, assuming one hydrogen atom on every surface Pt atom (Table 2). Accordingly, the amount of nitrite that could be converted if ammonia were the sole product [Eq. (2)] is 1.7 μmol (maximal consumption of $H_a$). If nitrogen were the sole product [Eq. (1)], then the amount of converted nitrite would be 3.3 μmol (minimal consumption of $H_a$). The conversion observed in our experiment (i.e., 2.4 μmol) lies between these boundary values, indicating formation of both ammonia and nitrogen. Unfortunately, these species could not be detected by MS because of their low molecular weight and stability compared with the relatively soft ESI ionization method. Nevertheless, the sensitivity of the MS detector allows quantitative determination of nitrite conversion caused by hydrogen coverage as low as 3%.

Fig. 8b shows the details of the responses to the nitrite pulse after all of the hydrogen was consumed. The striking difference in the shapes of the responses for $Pt/SiO_2$ and the support only clearly indicates a reversible and significant interaction of dissolved nitrite with the platinum surface. The step response indicates that about 0.05 μmol of nitrite adsorbed. This must have occurred on the Pt surface, because the results shown in Fig. 8b demonstrate the difference between the catalyst and the support only. The step-down response was less clear, in the sense that the amount of nitrite desorbed seemed smaller than the amount adsorbed; probably desorption occurred over a long period, after which the resulting nitrite signal could not longer be distinguished from the baseline. A strong interaction of nitrite with Pt was reported by Ebbesen et al. [39] in an ATR-IR study on adsorption of $NO_2^-$ on $Pd/Al_2O_3$ and $Pt/SiO_2$. Along with strong adsorption, our findings also indicate that reversible adsorption occurred as well. The amount was equivalent to 0.5% of a monolayer on platinum. We speculate that $NO_2^-$ interacted exclusively with a small fraction of specific sites at the surface of the Pt particles (e.g., corner sites). The remarkable sensitivity of the detector should be recognized at this point, allowing quantitative determination of nitrite adsorption of <0.01 monolayer (ML).

We observed a lower conversion of nitrite (i.e., 1.8 μmol) in subsequent $NO_2^-$ titration experiments, which implies a loss of platinum surface area. Furthermore, XRF analysis of the $Pt/SiO_2$ catalyst after three titration experiments showed a decrease in Pt loading (from 1.0 to 0.87 wt%). Hydrogen chemisorption of the $Pt/SiO_2$ catalyst after the titration experiments revealed a decrease in Pt dispersion from 0.65 to 0.58. These effects are possibly due to leaching of the smallest metal particles during the titration experiments; this would account for both the loss of Pt and the decrease in dispersion. Similar effects also have been reported by Douidah et al. [40] for small silica-supported platinum particles in aqueous media under hydrogen atmosphere.

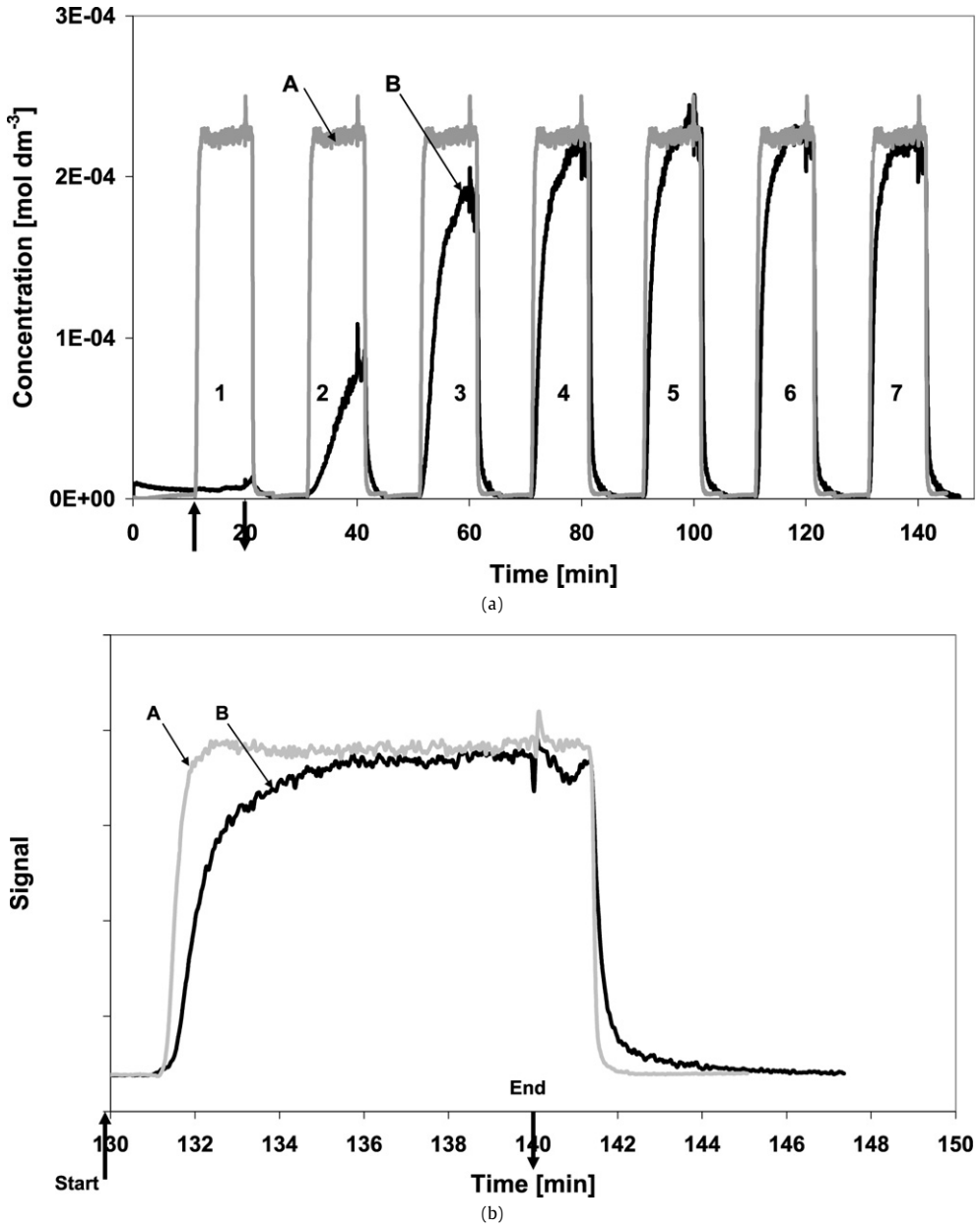


**Fig. 8.** (a) Titration of pre-adsorbed hydrogen on $Pt/SiO_2$ using pulses with nitrite aqueous solution (10 min long, 0.5 ml min$^{-1}$, $c_M = 2 \times 10^{-4}$ mol dm$^{-3}$ $NO_2^-$, $T = 60\,^\circ C$) over: (A) Reactor filled with silica and (B) reactor filled with $Pt/SiO_2$ catalyst with pre-adsorbed hydrogen. (b) Titration of pre-adsorbed hydrogen on $Pt/SiO_2$ using pulses with nitrite aqueous solution (10 min long, 0.5 ml min$^{-1}$, $c_M = 2 \times 10^{-4}$ mol dm$^{-3}$ $NO_2^-$, $T = 60\,^\circ C$) detail from pulse 7: (A) Reactor filled with silica and (B) reactor filled with $Pt/SiO_2$ catalyst with pre-adsorbed hydrogen.

In Part 2 of this paper we describe the development and application of a detector similar to membrane inlet mass spectrometry (MIMS) for online and real-time analysis of dissolved gases like $N_2$, to compensate for the ESI-MS detector's unsuitability in this respect.

### 3.5. Catalytic oxidation of glucose over a Pt/CNF/Ni supported on Ni foam

Fig. 9a shows the MS spectrum of the reactor effluent when a glucose solution was pulsed over Pt/CNF/Ni foam containing preadsorbed oxygen. A major part of the glucose was clearly converted, as demonstrated by the much lower peaks at m/z 215 and m/z 179 compared with those in the blank experiment shown in Fig. 5. The most significant peak in Fig. 9a, at m/z 195, was due to gluconic acid. Furthermore, peaks could be seen at m/z 177, 193, and 209 that were not found in the blank experiment, corresponding to fragments of side or intermediate products during glucose oxidation. These peaks can be assigned to glucose dialdehyde ($[C_6H_9O_6]^-$ at m/z 177) glucuronic acid ($[C_6H_9O_7]^-$ at m/z 193), and glucaric acid ($[C_6H_9O_8]^-$ at m/z 209), respectively [41].

Fig. 9b shows the results of repetitive pulsing with glucose on the preoxidized Pt/CNF/Ni catalyst. The left side of the figure compares the amount of remaining glucose (B) with the amount of glucose in the blank experiment in the absence of Pt (CNF-only, curve A); curve C shows the amount of gluconic acid formed. Clearly, glucose was converted to gluconic acid, and both the conversion and yield of gluconic acid decreased on repetitive pulsing, approaching zero on the fifth pulse. A total of 8.2 μmol of glucose was converted, whereas 5.6 μmol of gluconic acid was formed. The right side of Fig. 9b shows the response signal for the species

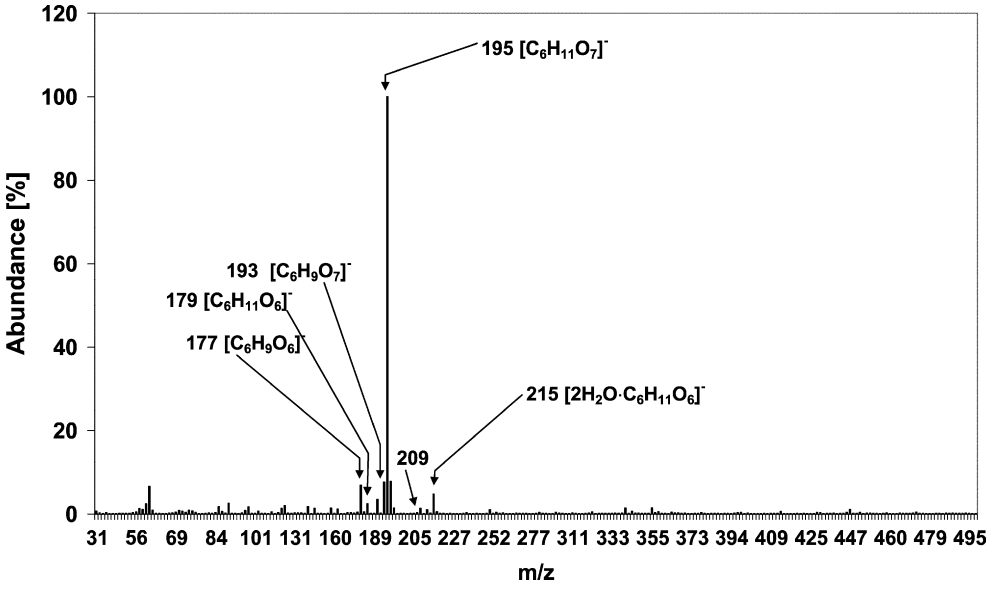


(a)

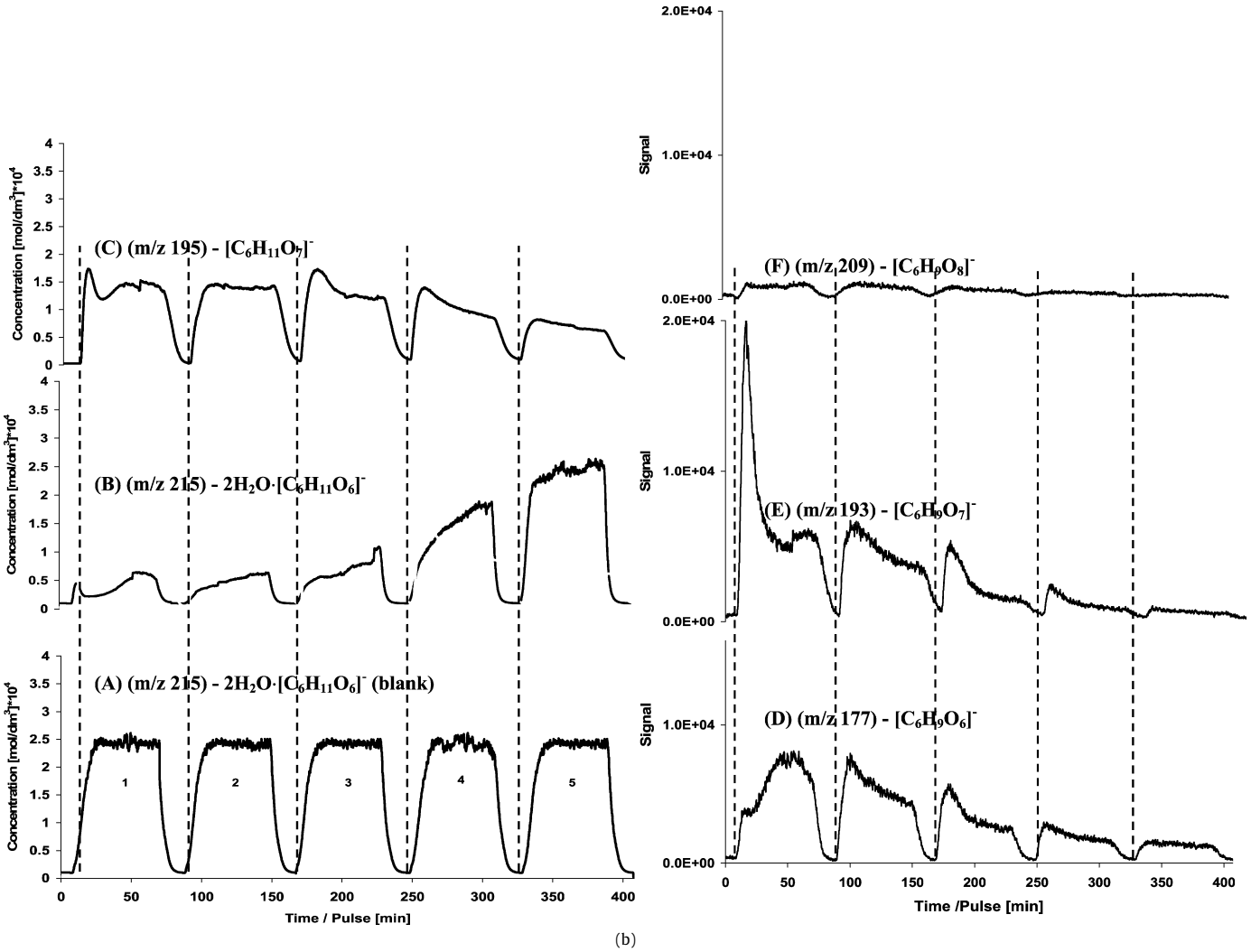


(b)

**Fig. 9.** (a) Spectrum from the first pulse during titration of pre-adsorbed oxygen on Pt/CNF catalyst with glucose from aqueous solution (pulse of 30 ml, 0.5 ml $min^{-1}$, $c_M = 5.6 \times 10^{-5}$ mol $dm^{-3}$, $T = 60\,^{\circ}C$). (b) Titration of oxygen pre-adsorbed on Pt/CNF supported on Ni-foam catalyst with the pulses of glucose aqueous solution (pulse of 30 ml, 0.5 ml $min^{-1}$, $c_M = 5.6 \times 10^{-5}$ mol $dm^{-3}$, $T = 60\,^{\circ}C$) reactor with CNF/Ni (A) glucose; reactor with Pt/CNF/Ni (B) glucose; (C) gluconic acid; (D) glucose dialdehyde; (E) glucuronic acid; (F) glucaric acid.

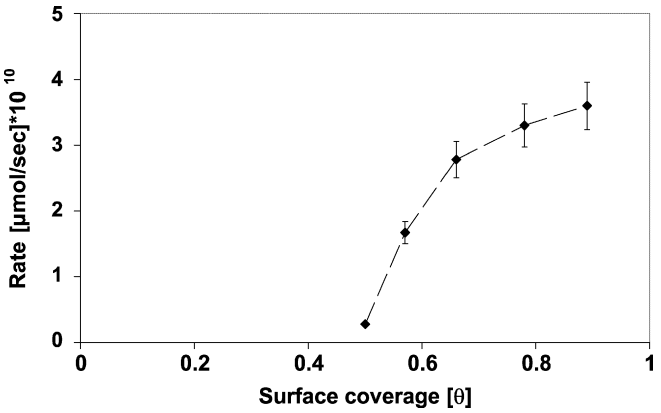


**Fig. 10.** Glucose oxidation reaction rate as function of the maximum estimate of the oxygen surface coverage ($\theta$).

with m/z 177, 193, and 209. Glucose dialdehyde and glucuronic acid clearly were formed; however, it should be noted that intensities of these signals were much lower than those for gluconic acid. Intensities decrease during repetitive pulsing. The peculiar differences in the shape of the first peak indicate that glucuronic acid was formed especially at very high oxygen coverage. It is not possible to discuss the shapes of the peaks in more detail, because chromatographic effects of the support are likely, as demonstrated by the fact that glucose adsorbs reversibly on silica. The mechanistic relevance of this observation is beyond the scope of this paper. The intensity of the signal due to glucaric acid was even lower, but the intensity remained significant, at least in the first few pulses.

The main reaction during selective oxidation of glucose can be described by the following equation:

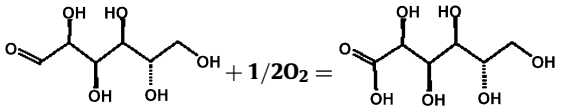


**Glucose** **Gluconic acid** (3)

The amount of oxygen available in the reactor was 10 µmol $O_a$ ($O_a$:$Pt_s$ = 1), and thus a maximum of 10 µmol of glucose could be converted to gluconic acid. The amount of glucose converted in our experiment (i.e., 8.2 µmol) was slightly less than this, and the amount of gluconic acid formed (i.e., 5.6 µmol) was even lower. The discrepancy between glucose converted and gluconic acid formed (i.e., 8.2 vs 5.6 µmol) is due, at least in part, to ionization suppression and charge competition effects between glucose and gluconic acid during ionization in ESI. In other words, calibration is influenced by the presence of the other species. Conversion to other products also may contribute somewhat, given the fact that traces of other compounds were detected, as discussed earlier.

Fig. 10 shows the relationship between the relative average reaction rate of glucose oxidation in each pulse (calculated based on the conversion level in each pulse) and the oxygen surface coverage. It is assumed that $O_a$:$Pt_s$ is equal to unity initially and that each glucose molecule reacts with only one preadsorbed oxygen atom. It should be noted that this procedure overestimates the oxygen coverage, because deep oxidation products also are formed (Fig. 9b). Unfortunately, quantifying these products is not possible; therefore, the oxygen surface coverages shown in Fig. 10 are just estimates, and the lowest oxygen coverage is probably <0.5 ML and may well be close to 0. Nevertheless, Fig. 10 shows decreasing reaction rates with decreasing oxygen coverage. This result demonstrates that in principle, the effect of O surface coverage on the reaction rate can be determined; however, a higher flow rate is needed to decrease the level of conversion to obtain the reaction order in adsorbed oxygen.

The novel technique introduced here performs better than existing transient techniques. The most significant advantage is the ESI-MS detector's ability to distinguish between different components, as was clearly demonstrated in the case of glucose oxidation. In contrast, RI and UV–vis detectors can follow only single compounds. In principle, ATR-IR also can distinguish between different compounds; however, IR absorption peaks must be well separated, which generally is not the case, and sensitivity is significantly lower. The response time of the detector allows detection in the range of 20 s, which is significantly faster then typical responses of the RI (range, 40 s for flows of 0.2–3 mL $min^{-1}$) or FTIR (range, 5 min for flows of 3–7 mL $min^{-1}$), underscoring the advantages of ESI-MS. The typical concentrations detected in our transient experiments ($10^{-6}$–$10^{-4}$ mol $dm^{-3}$) were significantly lower than those that can be detected by RI ($10^{-4}$–$10^{-2}$ mol $dm^{-3}$) or by FTIR ($10^{-2}$ mol $dm^{-3}$). The experiment with nitrite detected nitrite that visibly interacted with 0.01 ML Pt, demonstrating the advantages of the ESI-MS detector. Clearly, application of ESI-MS detection improved the sensitivity of the pulse-experiment significantly.

In summary, in both the experiments with glucose (converting adsorbed oxygen) and those with nitrite (converting adsorbed hydrogen), our technique allowed the detection of adsorbed species on Pt surface areas as small as 0.01 $m^2$. This remarkable sensitivity is very suitable for experiments using small amounts of catalysts in general, and thus our technique is promising for microreactors. We have demonstrated this for operation in the aqueous phase. In principle, application in the organic phase also is possible; however, the ESI-MS detector would need to be optimized for each specific application.

## 4. Conclusion

We have reported a novel, transient response technique for liquid-phase heterogeneous catalytic studies that was applied successfully for the first time. Our method is based on an online method for simultaneous detection of species dissolved in an aqueous stream at the exit of a catalytic reactor. ESI-MS was used for detection of dissolved molecules that readily ionize, as well as dissolved ions. Two test reactions, nitrite reduction with $Pt/SiO_2$ and glucose oxidation with Pt/CNF/Ni, were used to demonstrate semi-quantitative monitoring of reactants, intermediates, and products. The ESI-MS detector was demonstrated to be sufficiently sensitive to quantitatively determine very small amounts of physisorbing nitrite, down to 0.5% of a monolayer on the Pt surface. Nitrite also reacts with preadsorbed hydrogen, and the quantitative experimental results agree with the finding that both nitrogen and ammonia were formed. The ESI-MS detector is able to distinguish between different components simultaneously, as was demonstrated for glucose oxidation, providing its most significant advantage over existing transient techniques.

## Acknowledgments

The authors thank L. Vrielink for XRF and BET analysis, M. Smithers for TEM measurements, A. Hovestad for assistance with reactor preparation, and J. Spies and B. Geerdink for technical assistance. Financial support for the project (TPC 5694) by STW, The Netherlands is kindly acknowledged. This work was performed under the auspices of NIOK.

## References


[1] C.G.M. van de Moesdijk, The catalytic reduction of nitrate and nitric oxide to hydroxylamine: Kinetics and mechanism, Ph.D. thesis, University of Eindhoven, 1979.
[2] J.H. Clark, Pure Appl. Chem. 73 (2001) 103.
[3] J.W. Niemantsverdriet, Spectroscopy in Catalysis: An Introduction, Wiley–VCH, 2000, p. 5.
[4] H. Kobayashi, M. Kobayashi, Cat Rev. Sci. Eng. 10 (1974) 139.
[5] C.O. Bennet, M.B. Cutlip, C.C. Yang, Chem. Eng. Sci. 27 (1972) 2255.
[6] A.T. Bell, L.L. Hegedus (Eds.), ACS Symp. Ser., vol. 178, ACS, 1982, pp. 1–308.
[7] J.T. Gleaves, J.R. Ebner, T.C. Kuechler, Cat. Rev. Sci. Eng. 30 (1988) 49.
[8] G.S. Yablonsky, M. Olea, G.B. Marin, J. Catal. 216 (2003) 120.
[9] T.A. Nijhuis, L.J.P. van den Broeke, M.J.G. Linders, J.M. van de Graaf, F. Kapteijn, M. Makkee, J.A. Mouljin, Chem. Eng. Sci. 54 (1999) 4423.
[10] T. Bürgi, A. Baiker, J. Phys. Chem. B 106 (2002) 10649.
[11] S.D. Ebbesen, B.L. Mojet, L. Lefferts, J. Catal. 246 (2007) 66.
[12] J.F. Denayer, A. Bouyermaouen, G.V. Baron, Ind. Eng. Chem. Res. 37 (1998) 3691.
[13] G.H. Jonker, Hydrogenation of edible oils and fats, Ph.D. thesis, Rijksuniversiteit Groningen, 1999.
[14] V. Hejtmánek, P. Schneider, Chem. Eng. Sci. 49 (1994) 2575.
[15] Y. Lin, Y.H. Ma, Ind. Eng. Chem. Res. 28 (1989) 622.
[16] Z. Kiraly, A. Mastalir, A. Csaszar, H. Demir, D. Uner, G.H. Findenegg, J. Catal. 245 (2007) 267.
[17] F. Gao, K.P. Ng, C. Li, K.I. Krummel, A.D. Allian, M. Garland, J. Catal. 237 (2006) 49.
[18] D.K. Lloyd, in: W.J. Lough, I.W. Wainer (Eds.), High Performance Liquid Chromatography: Fundamental Principles and Practice, Blackie Academic & Professional, 1996, pp. 120–133.
[19] D.C. Harris, Quantitative Chemical Analysis, W.H. Freeman and Co., 2003, p. 517.
[20] http://www.agilent.com.
[21] D. Radivojević, K. Seshan, L. Lefferts, Appl. Catal. A 301 (2006) 51.
[22] N.A. Jarrah, J.G. van Ommen, L. Lefferts, J. Catal. 239 (2006) 460.
[23] S. Ebbesen, Spectroscopy under the surface—In-situ ATR-IR studies of heterogeneous catalysis in water, Ph.D. thesis, University of Twente, 2007.
[24] A. Pintar, Catal. Today 77 (2003) 451.
[25] M. Besson, P. Gallezot, Catal. Today 57 (2000) 127.
[26] H. Saito, O. Shinji, F. Shigeo, US Patent 4 843 173 (1989), to Kawaken Fine Chemical Corp. Ltd and Kao Corp.
[27] K. Deller, H. Krause, E. Peldszus, B. Despeyroux, US Patent 5 132 452 (1992), to Degussa.
[28] N.A.K.A. Jarrah, F. Li, J.G. van Ommen, L. Lefferts, J. Mater. Chem. 15 (2005) 1946.
[29] C.H. Bartholomew, R.J. Farrauto, Fundamentals of Industrial Catalytic Processes, Wiley–Interscience, 2006, p. 146.
[30] K.K. Unger, J. Chromatogr. Libr. 16 (1994) 53.
[31] P. Kebarle, Y. Ho, in: R.B. Cole (Ed.), Electrospray Ionization Mass Spectrometry—Fundamentals, Instrumentation and Applications, J. Wiley & Sons, Inc., 1997, p. 6.
[32] Y. Cai, M.C. Concha, J.S. Murray, R.B. Cole, J Am. Soc. Mass. Spectrom. 13 (2002) 1360.
[33] S. Gao, Z.-P. Zhang, H.T. Karnes, J. Chromatogr. B 825 (2005) 98.
[34] T. Mallat, A. Baiker, Catal. Today 19 (1994) 247.
[35] N.A.K.A. Jarah, Microstructured catalyst support based on carbon nano-fibers (CNFs), Ph.D. thesis, University of Twente, 2004.
[36] M.J. van Stipdonk, D.R. Justes, C.M. Force, E.A. Schweikert, Anal. Chem. 72 (2000) 2469.
[37] C.G. Enke, Anal. Chem. 69 (1997) 4885.
[38] M. D'Arino, F. Pinna, G. Strukul, Appl. Catal. B 53 (2004) 161.
[39] S.D. Ebbesen, B.L. Mojet, L. Lefferts, Langmuir 24 (2008) 869.
[40] A. Douidah, P. Marécot, J. Barbier, Appl. Catal. A 225 (2002) 11.
[41] S. Hermans, M. Devillers, Appl. Catal. A 235 (2002) 253.